

DDC FILE COPY

AD A059518

6
APPLICATION OF RAPID SOLIDIFICATION TECHNIQUES
TO ALUMINUM ALLOYS

10
Principal Investigator:
Professor R. Mehrabian
Department of Metallurgy and Mining Engineering
Department of Mechanical and Industrial Engineering
University of Illinois
Urbana, Illinois 61801
Tel.# (217) 333-2846

9 August, 1978
SIX MONTH TECHNICAL PROGRESS REPORT

Sponsored by:
DEFENSE ADVANCED RESEARCH PROJECTS AGENCY
ARPA Order Number: 3517
Contract Number: N00014-78-C-0275, ARPA Order-3517
Effective Date of Contract: 1 February 1978
Contract Expiration Date: 31 January 1980

Monitored by:
OFFICE OF NAVAL RESEARCH
Arlington, Virginia
Scientific Officer, Dr. B. A. MacDonald

This document has been approved
for public release and its
distribution is unlimited.

The views and conclusions contained in this document are those of the authors and should not be interpreted as necessarily representing the official policies, either expressed or implied, of the Defense Advanced Research Projects Agency or the U.S. Government.

78 09 08 006

175 750

JOE

SUMMARY

This program is being conducted for the purpose of developing a predictive model of heat flow and solidification for aluminum alloys produced under the high cooling rate conditions achievable in rotary atomization and laser surface melting. It is a combined experimental and theoretical study of the relationship between the important solidification variables (e.g. cooling rate, temperature gradients, interface shape and velocity, supercooling and transformation kinetics) and the structure and microchemistry of rapidly solidified aluminum alloys.

During the first six months of this program work was carried out in the following areas:

(a) A computer heat flow model for the rapid solidification of metal powders was developed.

(b) High purity Al-4.5% Cu alloy ingots were prepared and sent to United Technology Corporation for rotary atomization. Initial analysis of the structures of the metal powders produced were carried out.

(c) Generalized heat flow equations and computer codes were developed for one, two and three dimensional heat flow during rapid melting and subsequent solidification of a surface layer subjected to a high intensity heat flux, e.g. that generated by a continuous wave CO₂ laser.

(d) Substrates of Al-4.5% Cu alloy were specially prepared and sent to United Technology Corporation for surface melting. Initial characterization of the rapidly solidified specimens were carried out using electron microscope techniques.

Finally, a 15KW continuous wave CO₂ laser is presently being installed in our laboratories and should become available for use in this program in the near future.

ACCESSION FOR	
NTIS	W 14 Section <input checked="" type="checkbox"/>
DDC	B 3 Section <input type="checkbox"/>
UNANNOUNCED	<input type="checkbox"/>
POSTED	<input type="checkbox"/>
<i>on file</i>	
BY	
DISTRIBUTION/ATTN/DO NOT CITE	
A	

78 09 08 006

I. ATOMIZATION STUDIES

These studies are aimed at enhancing our current limited understanding of rapid solidification phenomena occurring during atomization of alloy powders by the centrifugal technique. It is now apparent that undercooling, nucleation and growth phenomena during rapid solidification can not always be explained with available theories of non-equilibrium dendritic solidification. For example, some centrifugally atomized powders show microcrystalline, non-dendritic, structures that can not be directly correlated to average cooling rate during solidification. Other phenomena, such as increased solid solubility, repression of non-equilibrium second phases and solute enriched dendritic cores are influenced by cooling rate prior to, as well as during solidification. Full exploitation of these observations in design of specific high strength alloy compositions for rapid solidification processing requires a much better understanding of the relationship between process variables - microstructure and microchemistry. While the specific emphasis of the work in this program is on aluminum alloy powders produced by centrifugal (rotary) atomization, the findings should be applicable to other alloy systems and atomization processes.

In the first six months of this program a comprehensive literature survey was initiated and both theoretical and experimental studies were carried out on rapid solidification of aluminum alloy powders. Initial findings from this work are presented below.

1. Literature Survey

The literature survey initiated was on the reported effects of rapid solidification on the microstructural modifications of aluminum alloys, as well as the theoretical models available that

relate high cooling rates to nucleation and transformation kinetics during crystalline solidification. Results of the reported microstructural modifications would be used to both select specific aluminum alloys for this study and to relate and compare the effect of calculated achievable cooling rates in rotary atomization on structure and microchemistry with other rapid solidification processes. Reported microstructural modifications of aluminum alloys due to rapid solidification can be summarized as follows:

- a) Microstructural refinement, manifested as smaller grain size and dendrite arm spacings.
- b) Extension in terminal solid solubility of the primary α -Al phase.
- c) Morphological changes of the eutectic or the primary phase.
- d) Formation of non-equilibrium phases.
- e) Coupled eutectic growth at off-eutectic compositions.
- f) Vacancy super saturation.

Reported extensions of solid solubility and non-equilibrium second phases detected in binary aluminum alloys are summarized in Tables I and II, respectively. A review of these data and practical considerations based on present and future commercial alloys for rapid solidification applications indicate Al-Cu, Al-Fe and Al-Si systems to be most promising for fundamental atomization studies.

2. Theoretical Studies

The initial studies in this portion of the program were aimed at developing a versatile computer heat flow model for solidification of atomized droplets of both single melting point metals and

TABLE I

Extension of Solid Solubility in Binary Aluminum
Alloys Quenched from the Melt*

Element	Max. at equil.		Reported Maximum
	at%	Temp. °K	at - %
Cr	0.44	934	>5-6
Cu	2.5	821	17-18
Fe	0.025	928	4-6
Mg	18.9	723	36.8-40
Mn	0.7	923	>6-9
Ni	0.023	913	1.2-7.7
Si	1.59	850	10-16
Zn	66.5	655	38 ?

* From reference # 1

TABLE II

Non Equilibrium Phases Detected in Aluminum Binary Alloys Under Rapid Solidification

Alloying Element	Concentration Range (at%)	Non-Equilibrium Phase detected	Type	Corresponding Eq. Phases	References
Cr	1.6-3	Al_4Cr	I	$\alpha-Al + Al_7Cr$	2
Cu	45	Al_3Cu_2 (Trigonal)	III	$\theta + \eta_2$	3
	17.3	Noncrystalline	III	$\alpha-Al + \theta$	4
Fe	2-4	$\gamma, \gamma', \gamma'', \theta^\dagger$	II	$Al_3Fe + \alpha-Al$	5
	4	Al_6Fe (Orthorhombic)	II		6
		Al_6Fe	III		7
Mg	25	$L2_2$ superlattice	II	$\alpha-Al + \beta-Al_3Mg_2$	1
	40	($\alpha-Mn$) like structure	III	$\alpha-Al + \beta-Al_3Mg_2$	1
Mn	≤ 6	Al_4Mn	I	$\alpha-Al + Al_6Mn$	7
Ni	7.3-10.1	η (Orthorhombic)	III	$\alpha-Al + \beta-Al_3Ni$	8

[†] Formed transiently during aging following a decomposition kinetics similar to the supersaturated Al-Cu solid solutions.

alloys that freeze over a range of temperatures. A generalized computer code was developed for the former and will be described herein, while work on the alloy system is presently underway and will be reported in the future.

The computer heat flow model developed for solidification of pure metals and alloys that freeze at a single temperature permits prediction of the important solidification variables (e.g. cooling rate, interface velocity, temperature gradient, etc.) as a function of the dimensionless variables governing the rate of heat extraction from metal droplets. A manuscript based on this work is in preparation. A short summary of some of the important findings is as follows.

In general, the achievable heat transfer coefficients at a liquid metal droplet-environment interface are limited to $h < 10^5$ W/m².K.⁽⁹⁾ For aluminum metal droplets in the size range of $\sim 1\mu\text{m}$ to $1000\mu\text{m}$ this translates to a limitation on the range of Biot Numbers of interest, $10^{-2} > Bi > 1.0$.

$$Bi = \frac{hr_0}{k_L} \quad (1)$$

where h is the heat transfer coefficient of the metal droplet-environment interface, r_0 is the radius of the droplet and k_L is the conductivity of the liquid metal.

Figure 1 shows calculated dimensionless temperature versus dimensionless distance in a liquid aluminum metal droplet for various Biot Numbers at the instant its surface reaches the melting point. The data shows that for Biot Numbers less than ~ 0.01 there is no significant temperature gradient in the droplet and the simple

Newtonian cooling expressions can be used.

An important variable effecting supercooling prior to nucleation is the cooling rate in the liquid droplet. A generalized expression relating the instantaneous average cooline rate, ϵ_{avg} , in a liquid metal droplet to the Biot Number and dimensionless surface temperature was derived:

$$\epsilon_{avg} = 3 \times Bi \times \theta_{SURFACE}$$

where:

$$\epsilon_{avg} = -3 \int_0^1 \rho^2 \left(\frac{d\theta}{dFo} \right) d\rho \quad (2)$$

$$\rho = \frac{r}{r_o}$$

$$\theta = \frac{T - T_g}{T_m - T_g}$$

$$Fo = \frac{\alpha_L t^2}{r_o^2}$$

T = temperature in the droplet

T_g = temperature of the environment

T_m = melting point of the droplet

α_L = thermal diffusivity of the liquid metal

t = time

Computer calculations show that dimensionless solidification interface velocity $\partial \rho_L / \partial (Fo)$ increases with both increasing Biot Number and with distance solidified from the droplet surface at a given Biot Number, Figure 2.

Examples of the type of numbers which can be generated from the data presented in equation (2) and Figure (2) are as follows. A 50 μ m diameter aluminum droplet convectively cooled with a high velocity gas environment, as in the centrifugal atomization process

of the United Technologies Corporation, may achieve a surface conductance (surface heat transfer coefficient) of $h \sim 5 \times 10^4 \text{ W/m}^2 \cdot ^\circ\text{K}$. The calculated average cooling rate in the liquid droplet from equation (2) when its surface reaches the melting point is $\sim 1.4 \times 10^6 \text{ }^\circ\text{K/sec}$. The solid-liquid interface velocities, from Figure 2, at radius ratios of 0.95 and 0.25 are 0.037 m/sec and 0.32 m/sec, respectively.

As noted above, a new heat flow model is presently being developed for solidification of alloys that freeze over a range of temperatures, hence liquid compositions.

3. Experimental Studies

Several high purity ingots of Al-4.5% Cu alloy weighing approximately 2 kilograms were prepared in our laboratories and sent to United Technologies Corporation. Two of the ingots were remelted, centrifugally atomized and solidified by forced convective cooling. The resulting powders are being subjected to microstructural analysis using various electron microscope techniques. Figure 3 shows the three distinct types of structures noted to date. The micrograph in Figure 3(b) shows typical dendritic structures found in the atomized droplets. Average measured dendrite arm spacings are of the order of $\sim 2 \text{ } \mu\text{m}$. The micrograph in Figure 3(c) shows a duplex microstructure - primary spheroidal solid particles surrounded by a fine dendritic matrix. This structure is very similar to that obtained when a metal alloy is subjected to high rates of shear during initial stages of solidification - Rheocast structures (10). It is postulated that these droplets partially solidified on the disk of the rotary atomizer prior to flight into the forced convective cooling environment. On the other hand, the

powder particle in Figure 3(a) also shows a duplex structure which is similar to Figure 3(c) yet, it is significantly different in its response to etchants and its general appearance in the Scanning Electron Microscope.

Detailed structural and microchemical analysis of these structures is presently underway. Techniques are being developed for the preparation of electron transparent specimens of the powder cross-sections for Scanning and Conventional Transmission Electron Microscope Studies.

Ingots of high purity Al-Fe and Al-Si alloys are also being prepared in our laboratories for centrifugal atomization at the United Technologies Corporation.

II. LASER SURFACE MELTING

A corollary theoretical and experimental program was undertaken to investigate rapid surface melting and subsequent solidification of aluminum alloy substrates subjected to high intensity heat fluxes such as that generated by continuous wave CO_2 lasers. The two features of rapid surface melting which make it an attractive tool to correlate rapidly solidified structures to solidification variables are:

- (a) Theoretical heat flow calculations can be carried out without recourse to arbitrary assumption of a heat transfer coefficient between the liquid and the substrate below - there is intimate contact between the two.
- (b) It separates growth phenomena from nucleation events in rapid solidification processing - special substrates can be prepared for epitaxial growth studies.

Our investigations are aimed at coupling computed heat flow conditions with experimentally observed microstructures in the aluminum alloys used for the centrifugal atomization studies. Heretofore, laser surface melting of our aluminum substrates was carried out at the United Technologies Corporation. Recently, a 15KW continuous wave CO_2 laser was acquired by the University of Illinois and is presently being installed in our laboratories. It is anticipated that specimens would also be surface melted with this new in-house facility.

1. Heat Flow Calculations

Generalized heat flow equations and computer codes were developed for prediction of the important rapid melting and subsequent solidification variables of surface layers subjected to high intensity

heat fluxes. Specific work carried out in the first six months of this program is summarized below.

(a) One-Dimensional Heat Flow

Numerical calculations of a one-dimensional heat flow model developed earlier were completed and published during this contract period. The original manuscript submitted for publication prior to this contract was revised to include these recent calculations. The published manuscript is attached hereto as an Appendix.

Shortcomings of this work included assumptions of uniform absorbed heat flux and one-dimensional heat flow - it is assumed that the laser spot diameter is large in comparison with the heat affected zone in the substrate.

(b) Two-Dimensional Heat Flow

In this study we have developed generalized expressions for the finite difference coefficients of the energy conservation equation in a curvilinear coordinate system. We have considered the rapid melting and subsequent solidification of the surface layer of a semi-infinite aluminum substrate, initially at room temperature, subjected to a high intensity heat flux over a circular region on its bonding surface. Both uniform and Gaussian distributions of the absorbed heat flux were considered. However, the equations and computer codes developed can treat any arbitrary heat flux over the circular region.

Computer calculations are presently underway for a range of absorbed heat flux and the results of the computations are being compared with the one-dimensional heat flow model. Figure 4 shows the calculated fractional melt depths (liquid-solid interface positions) at various times during surface melting of an aluminum

substrate subjected to a uniform absorbed heat flux of $5 \times 10^9 \text{ W.m}^{-2}$. The two sets of curves are for different laser spot radii, 190 μm and 380 μm . Figure 5 shows similar data obtained for two different absorbed heat fluxes. The data in Figures 4 and 5 indicate that some of the general relationships developed between absorbed heat flux, melt depth and time in the one-dimensional model (see Appendix) may also hold for the two-dimensional transient heat flow model.

It is anticipated that data generated in the next two months would permit the development of specific relationships between absorbed heat flux and isotherm shapes, isotherm velocities and temperature gradients. Experiments are also planned in which the conditions for these two-dimensional transient heat flow calculations can be simulated by laser radiation of stationary aluminum substrates.

(c) Three-Dimensional Heat Flow

In this work we have addressed the problem of rapid surface melting and subsequent solidification of a semi-infinite solid, moving with constant velocity, subjected to a high intensity heat flux over a circular region of its bonding surface. Temperature profiles in the molten region and the adjacent heat affected zone, as well as the important melting and solidification variables are to be determined.

Generalized expressions for the coefficients of the finite difference equations governing heat transfer in discretized spatial domains in moving curvilinear systems have been developed along with a computer code for numerical solutions. Initial data obtained show that the method used is accurate and does lend itself to solution of this multi-dimensional phase change problem. It is anticipated that this investigation would be completed in the

next six months of this program.

Solution of the problem described above should accurately simulate the thermal field geometries encountered in laser surface melting of moving substrates. This is the technique presently used in our experimental work. Finally, the general expressions and solution techniques developed should also be applicable to calculation of thermal fields and solidification parameters in the metal pool of certain types of welding processes.

2. Experimental Studies

Unidirectional ingots of Al-4.5% Cu alloy were cast and sectioned into appropriate sizes for laser surface melting. These were surface melted at United Technologies Corporation under conditions predicted from the heat flow studies to yield a range of melt depths and solidification conditions. Preliminary examination of the structures obtained via SEM and Conventional TEM techniques has been completed. Figure 6 shows representative TEM photomicrographs of one laser melted specimen. As anticipated, the structures are very fine and are aligned in the heat flow direction. Work is now underway to determine composition profiles across the fine segregate spacings via STEM. Correlation of structures and microchemistries to calculated heat flow conditions and solidification - segregation models would be an important aspect of this work in the future.

Presently, special single crystal specimens of aluminum alloys are being grown in our laboratories for laser surface melting studies. It is expected that epitaxial growth studies could be better carried out on these substrates.

MANUSCRIPTS PREPARED OR IN PREPARATION
BASED ON WORK IN THIS PROGRAM

1. S - C. Hsu, S. Chakravorty, R. Mehrabian, "Rapid Melting and Solidification of a Surface Layer," Met. Trans. B., Vol. 9B, June 1978, p. 221.
2. R. Mehrabian, S - C. Hsu, C. Levi, S. Kou, "Heat Flow in Rapid Solidification," Proceedings of 25th Sagamore Army Materials Conference, 17-21, July, 1978, Bolton Landing, New York. To be published by Syracuse Press.
3. S - C. Hsu, S. Kou, R. Mehrabian, "Rapid Melting and Solidification of a Surface Layer - Two-Dimensional Heat Flow." To be submitted to Metallurgical Transactions.
4. S. Kou, S-C. Hsu, R. Mehrabian, "Rapid Melting and Solidification of a Surface Layer Subjected to a High Intensity Moving Heat Flux." To be submitted to Metallurgical Transactions.
5. C. Levi, R. Mehrabian, "Heat Flow During Solidification of Atomized Droplets." To be submitted to Metallurgical Transactions.
6. R. Mehrabian, S. Kou, S-C. Hsu, "Laser Surface Melting and Solidification." Invited lecture to be published in the Proceedings of Symposium on Laser - Solid Interactions and Laser Processing, Nov. 28-Dec. 1, 1978, Boston, Mass.
7. S-C. Hsu, S. Kou, R. Mehrabian, "Heat Flow in Laser Processing," to be published in Proceedings of ASM Conference on Applications of Lasers to Materials Processing, April 18-20, 1979, Washinton, D.C.

REFERENCES

1. H. Jones, "Developments in Aluminum Alloys by Solidification at Higher Cooling Rates." To be published in Aluminium.
2. N. I. Varich and R. B. Lyukevich, Russ. Met., 1970, Vol. 4, p. 58.
3. P. Ramachandrarao and M. Lavidjani, J. Mater. Sci., 1974, Vol. 9, p. 434.
4. H. A. Davies and J. B. Hull, J. Mat. Sci., 1974, Vol. 9, p. 707.
5. E. Blank, Z. Metallkunde, 1972, Vol. 63, p. 324.
6. M. H. Jacobs, A. G. Doggett and M. J. Stowell, J. Mater. Sci., 1974, Vol. 9, p. 1631.
7. N. I. Varich and K. Ye. Kolesnichenko, Met. Abs., 1961, Vol. 28, p. 715.
8. A. Tonejc, D. Rocak and A. Bonefacic, Acta. Met., 1971, Vol. 19, p. 311.
9. R. Mehrabian, Proceedings of Conference on Rapid Solidification Processing: Principles and Technologies, Editors, R. Mehrabian, B. H. Kear and M. Cohen, Claiborne's Publishing Div., Baton Rouge, Louisiana, 1978.
10. S. D. E. Ramati, G. J. Abbaschian and R. Mehrabian, Met. Trans. B., 1978, Vol. 9B, p. 241.

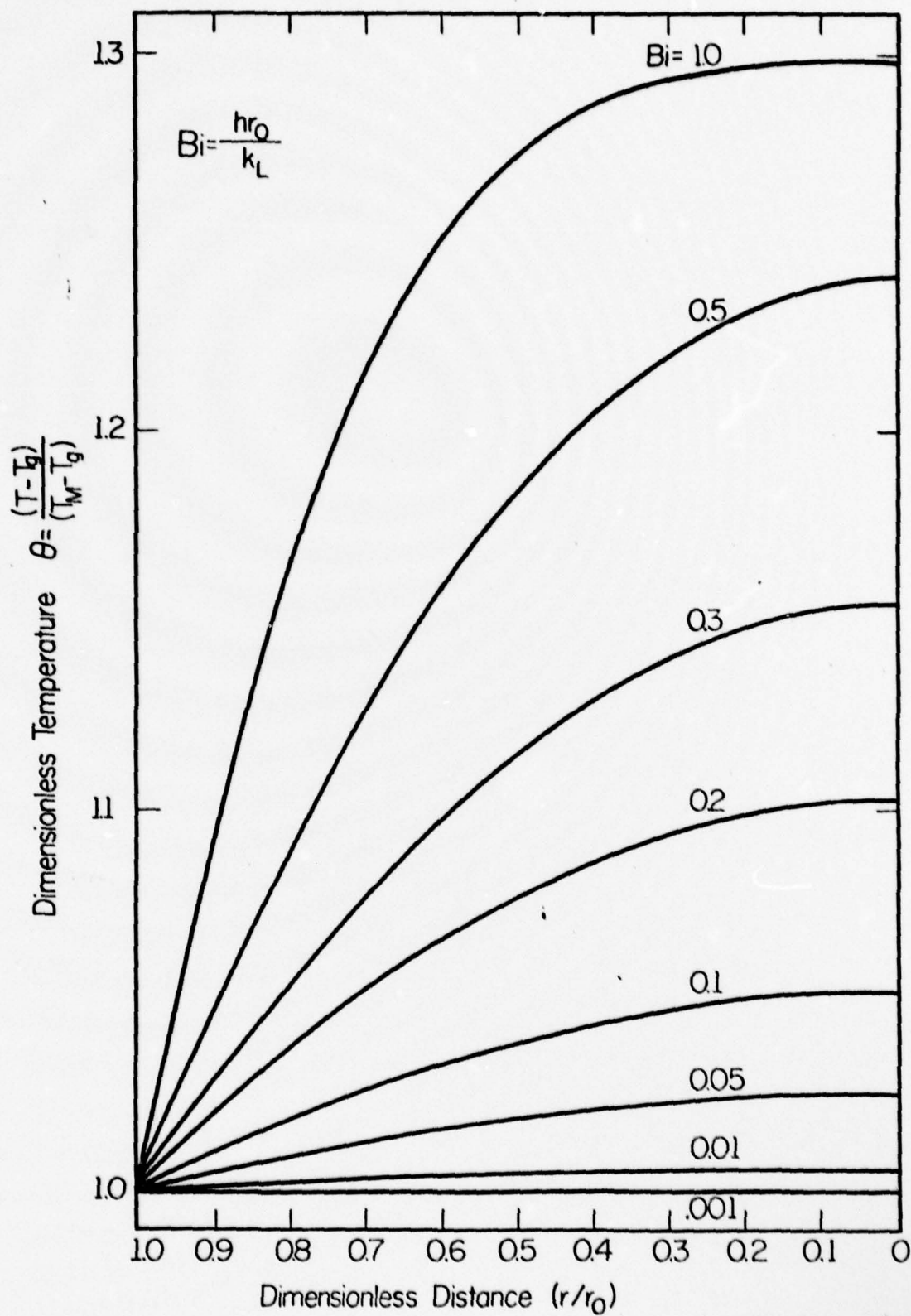


Figure 1 Calculated dimensionless temperature versus dimensionless distance in liquid droplets of aluminum for different Biot Numbers.

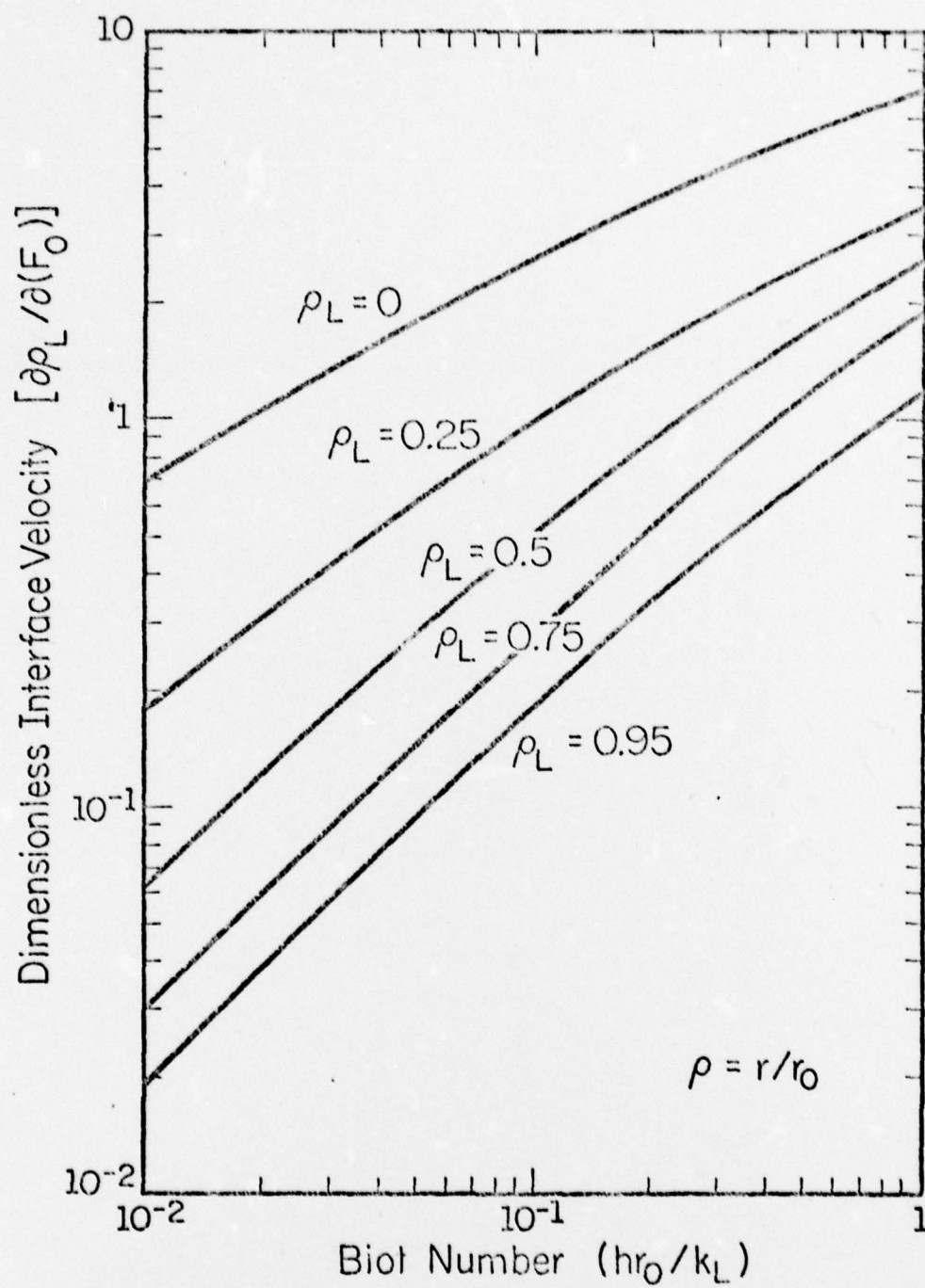


Figure 2. Dimensionless solid-liquid interface velocity versus Biot Number during solidification of aluminum powders at different interface positions.

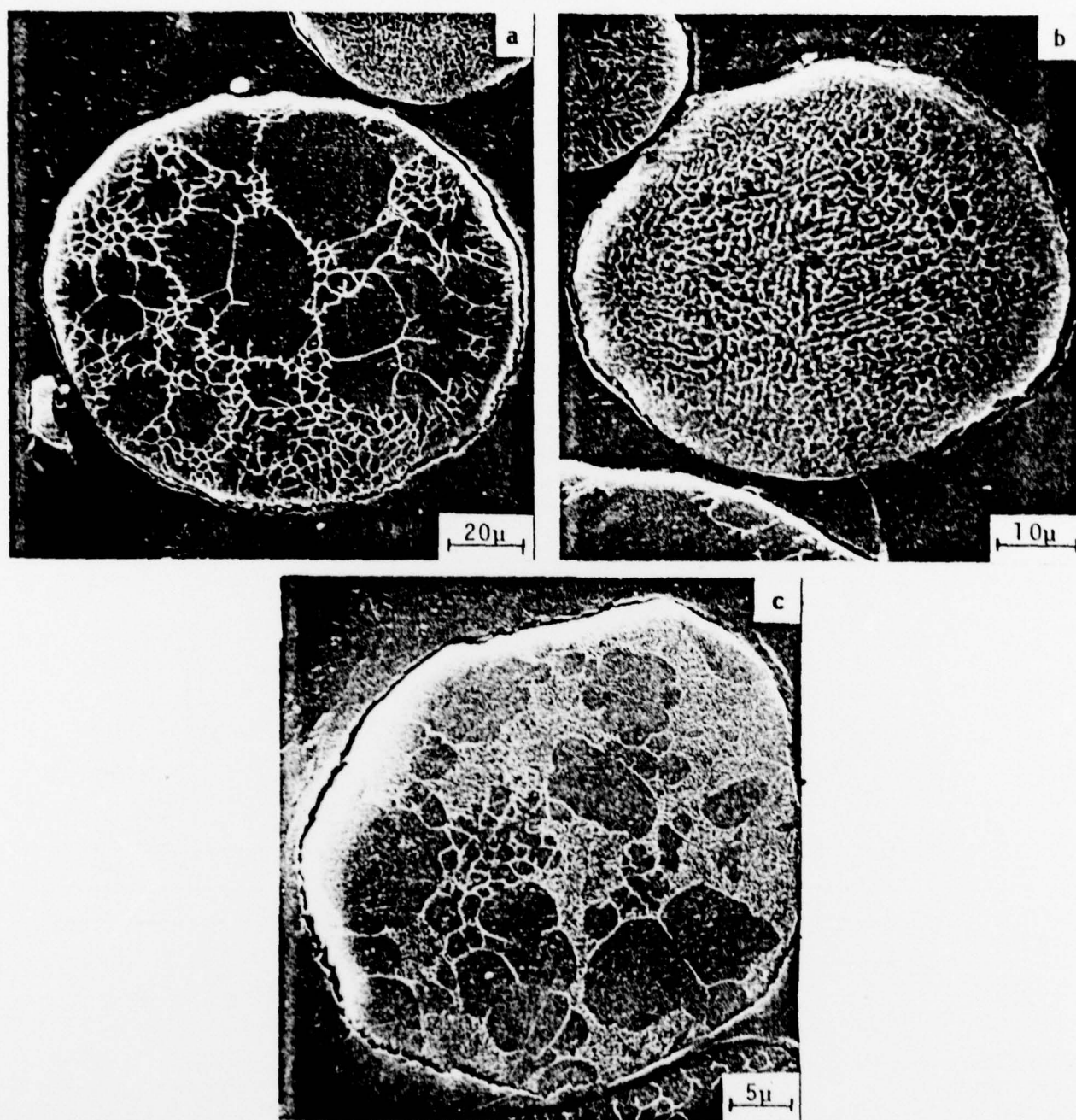


Figure 3 Scanning Electron Micrographs of three distinct microstructures observed in Al-4.5% Cu alloy powders produced by the centrifugal atomization technique.

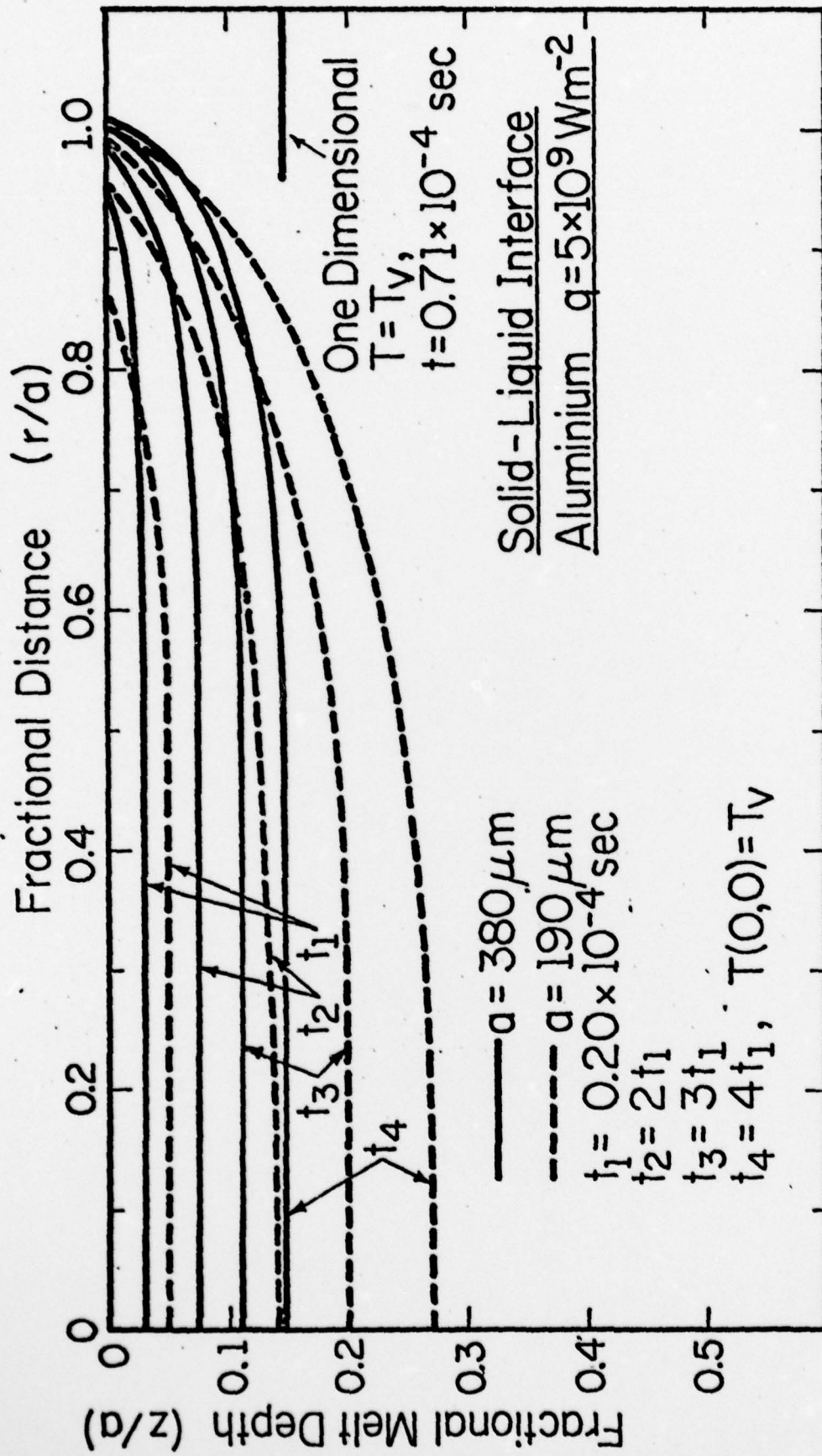


Figure 4 Calculated liquid-solid interface positions at various times in the laser surface melted region of an aluminum substrate. Absorbed heat flux is $5 \times 10^9 \text{ Wm}^{-2}$. The two sets of curves are for laser spot radii of $190 \mu\text{m}$ and $380 \mu\text{m}$, respectively. $T(0,0) = T_V$ curves denote times when the center of the circular region on the bonding surface reaches the vaporization temperature.

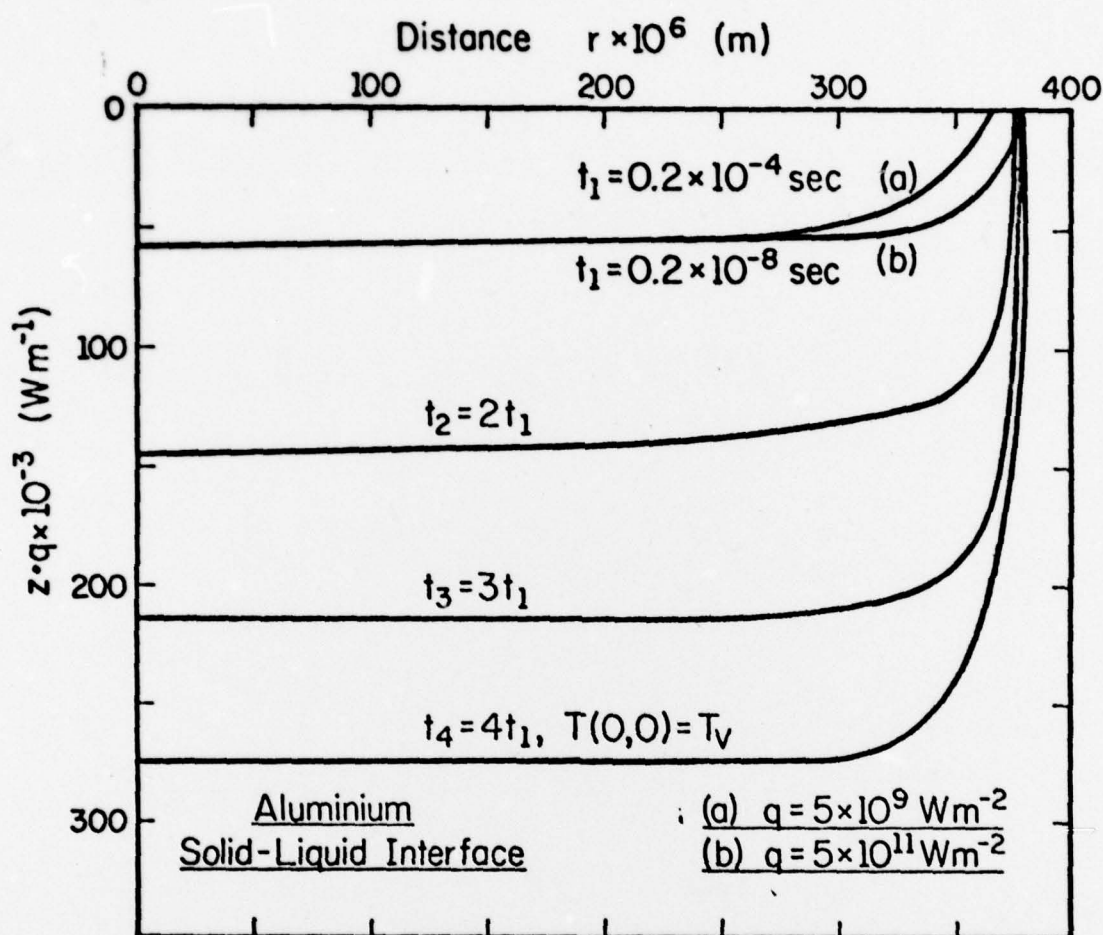


Figure 5 Calculated liquid-solid interface positions at various times in the laser surface melted region of an aluminum substrate for two different absorbed heat fluxes. Laser spot radius was assumed to be $380 \mu\text{m}$.



Figure 6 TEM photomicrographs of laser melted surface of an Al-4.5% Cu alloy substrate.

Rapid Melting and Solidification of a Surface Layer

S. C. HSU, S. CHAKRAVORTY, AND R. MEHRABIAN

A one-dimensional computer heat flow model is used to investigate the effect of high intensity heat fluxes, *e.g.* those achieved via continuous CO₂ laser radiation, on the important surface layer melting and subsequent solidification variables of three substrate materials: aluminum, iron, and nickel. Temperature profiles *vs* time, melting, and solidification interface velocities, heating, and cooling rates in the surface layers of the three metals are calculated. Results are presented in a general form to permit determination of these variables for large ranges of absorbed heat fluxes and times. General trends established show that temperature gradients in the liquid and solid phases and interface velocities are directly proportional to the absorbed heat flux, whereas melt depth is inversely proportional to the absorbed heat flux. Average cooling rates comparable to splat cooling can be achieved by increasing the heat flux and reducing the dwell time of the incident radiation. An order of magnitude increase in the absorbed heat flux results in a corresponding two orders of magnitude increase in average cooling rates in the liquid during solidification of crystalline and noncrystalline structures.

I. INTRODUCTION

THE effect of high cooling rates, 10^5 to 10^{10} K/s on the structure of solid materials formed from their melts has received increased attention ever since Duwez and his coworkers published results of their investigations on splat cooling.^{1,2} A large number of innovative batch and continuous techniques for production of laboratory and commercial quantities of rapidly solidified material have since been developed. In general, these techniques involve quenching of a liquid on a high conductivity substrate. Determination of exact cooling rates during solidification of crystalline and noncrystalline structures in these processes has required estimates of heat transfer coefficients between the liquid and the substrate. Two noteworthy attempts have been made to directly measure heat transfer coefficients during splat cooling.^{3,4} However, it is questionable whether these values can be used in calculation of cooling rates in other rapid solidification techniques or even in splat cooling in general because of different processing conditions, alloy compositions and substrate materials.

The recent availability of high power continuous wave, CO₂ laser has led to the development of a rapid surface melting and solidification technique⁵ in which the bulk (semiinfinite) substrate in intimate contact with the molten layer acts as the quenching medium—an infinite heat transfer coefficient can be assumed. This paper describes a theoretical study carried out to investigate the effect of high intensity radiation on the important surface layer melting and subsequent

solidification variables of three substrate materials: aluminum, iron, and nickel.

Several studies have previously been carried out to quantitatively describe heat flow in a semiinfinite substrate material subjected to high intensity radiation. An analog computer program was developed by Cohen⁶ to investigate the temperature distributions in the molten surface layer and the solid substrate during melting of a semiinfinite solid subjected to a step-function heat input. The thermal profiles thus generated were subsequently used by other investigators to estimate average cooling rates during solidification of noncrystalline structures.⁵ Other researchers⁷ have used the point source heat flow equations proposed by Rosenthal⁸ for bead-on plate welding. One difficulty with all theoretical calculations, including that presented here, is that not all incident radiation is absorbed by the substrate—reflectivity varies with power density, substrate material, surface condition (*e.g.*, oxide layer), and is different for primary phases and inclusions. Nevertheless, it was believed that a detailed study of the thermal characteristics of pure substrate materials would yield useful relationships between the absorbed heat flux and the important melting and solidification variables influencing structure.

In practice, dwell time of an incident radiation can be calculated from the scanning speed and spot diameter of the incident beam.^{5,7} The one-dimensional heat flow model used in this study assumes that the spot diameter is large in comparison with the melt depth. Furthermore, it is assumed that there is no convection in the molten surface layer. The effect of convection on melt depth was determined by arbitrarily increasing the conductivity of the liquid. In the extreme, the conductivity of a well mixed liquid tends to infinity and analytical equations developed by Landau⁹ for complete removal of the melt could be applied. In lieu of exact analytical solutions for the problem at hand, approximate analytical techniques such as the "approximate integral technique" developed by Goodman¹⁰ can be used. Melt depth calculations based on this latter approach were also carried out in this study and are compared to those calculated via the numerical integration technique.

S. C. HSU is Graduate Research Assistant, Department of Mechanical and Industrial Engineering, University of Illinois, Urbana-Champaign, Illinois. S. CHAKRAVORTY, formerly Research Associate, Department of Metallurgy and Mining Engineering, University of Illinois, Urbana-Champaign, Illinois, is now Assistant Professor, Department of Materials Science and Engineering, Pahlavi University, Shiraz, Iran. R. MEHRABIAN is Associate Professor, Department of Metallurgy and Mining Engineering and Department of Mechanical and Industrial Engineering, University of Illinois, Urbana-Champaign, Illinois.

Manuscript submitted July 11, 1977.

Table I. Summary of Properties and Numerically Calculated Constants

Element	Solid Density, ρ_s Kg m ⁻³	Liquid Density, ρ_l Kg m ⁻³	Melting Temperature, T_M K	Boiling Temperature, T_v K	Thermal Conductivity of Solid, k_s J s ⁻¹ m ⁻¹ K ⁻¹	Thermal Conductivity of Liquid, k_l J s ⁻¹ m ⁻¹ K ⁻¹
Aluminum	2700	2390	933	2723	228*	108†
Iron	7860	7030	1808	3273	42*	44†
Nickel	8900	7900	1728	3005	74*	43
Element	Specific Heat of Solid, C_{ps} J Kg ⁻¹ K ⁻¹	Specific Heat of Liquid, C_{pl} J Kg ⁻¹ K ⁻¹	Thermal Diffusivity of Solid, α_s m ² s ⁻¹	Thermal Diffusivity of Liquid, α_l m ² s ⁻¹	Latent Heat of Fusion, H J Kg ⁻¹	$\frac{L + S}{L_{max}}$
Aluminum	1048*	1086†	8.1×10^{-5}	4.2×10^{-5}	3.95×10^5	9.3
Iron	691*	628†	7.7×10^{-6}	1.0×10^{-5}	2.72×10^5	12.2
Nickel	556*	656†	1.5×10^{-5}	8.3×10^{-6}	2.99×10^5	21.6
Element	$\frac{q\sqrt{t_m}}{J m^{-2} s^{1/2}}$	$\frac{q\sqrt{t_v}}{J m^{-2} s^{1/2}}$	$\frac{q\sqrt{t_{max}}}{J m^{-2} s^{1/2}}$	$\frac{\rho_l H}{\rho_s C_{ps}(T_M - T_0)}$	$\frac{(T_v - T_M)C_{pl}}{H}$	$\frac{\sqrt{\pi/2} \sqrt{k_s \rho_s C_{ps}} (T_M - T_0)}{J m^{-2} s^{1/2}}$
Aluminum	1.43×10^7	4.21×10^7	5.19×10^7	0.53	4.92	1.43×10^7
Iron	2.02×10^7	4.07×10^7	4.26×10^7	0.23	3.38	2.02×10^7
Nickel	2.43×10^7	4.27×10^7	4.41×10^7	0.33	2.80	2.43×10^7

*Averaged from 298 K to M.P.

†Averaged from M.P. to B.P.

II. HEATING OF THE SOLID

The temperature distribution in a semiinfinite solid subjected to a constant heat flux at its surface is readily determined from equations given in Carslaw and Jaeger.¹¹ These equations were used to establish the initial temperature distributions *vs* time in the different substrates prior to surface melting. The product of $q\sqrt{t_m}$, where q and t_m are absorbed heat flux and time for the surface of the solid to reach its melting point, respectively, is a constant for a given material. The calculated values of this constant and all other properties of the three elements (aluminum, nickel and iron) used in this study are listed in Table I.

Data thus generated were used both in the determination of melt depths *vs* time via the approximate integral technique and to establish initial temperature profiles for the numerical calculations.

III. APPROXIMATE INTEGRAL TECHNIQUE

Integration of the one-dimensional transient heat conduction equation for the case of a semiinfinite solid at its melting point subjected to a constant heat flux at its surface leads to a heat balance integral given by Goodman.¹⁰ Solution of this integral with the appropriate boundary conditions at the surface of the metal and the liquid-solid interface is facilitated by an *a priori* assumption of a temperature distribution in the liquid. In this work the temperature distribution in the liquid was represented by a quadratic equation and the analytical solutions to the heat balance integral derived by Evans *et al*¹² for this case were used to generate curves of maximum melt depth, L_{max} , *vs* absorbed heat flux. The maximum melt depth throughout this paper refers to the melt depth achieved for a given absorbed heat flux when the surface of the material reaches its vaporization temperature, T_v , and the heat flux is removed.*

*See Nomenclature for definition of all notations.

Figure 1 shows calculated maximum melt depths *vs* absorbed heat flux for the three elements. The more precise calculations using the computer model discussed in the next section are also shown in the same figure. The procedure outlined above, while providing useful order of magnitude estimates of melt depths, has severe shortcomings. It does not permit determination of temperature profiles in the solid; therefore, it cannot be used for calculation of thermal profiles during solidification of the molten surface layer once the heat flux is removed.

IV. COMPUTER SOLUTION

The numerical integration, finite difference method, developed by Murray and Landis¹³ was used for both the melting and subsequent solidification of a surface layer subjected to a constant heat flux for a given period of time. Initial conditions were established us-

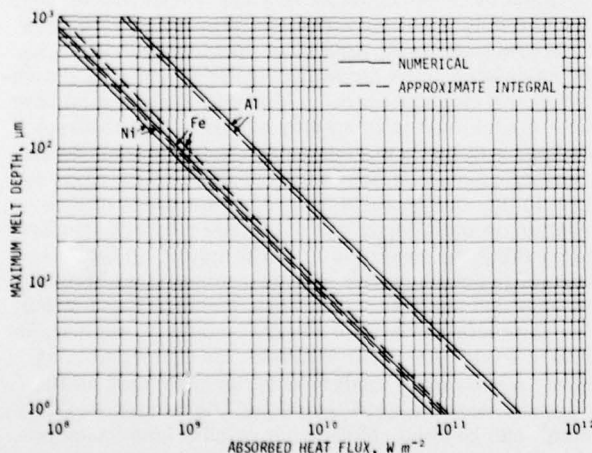


Fig. 1—Maximum melt depth *vs* absorbed heat flux for aluminum, iron and nickel calculated using the approximate integral and numerical techniques.

ing data generated from analytical expressions discussed earlier for the single phase solid material. Natural convection due to buoyancy forces in the liquid and fluid motion due to density differences in the two phases were ignored.* Pure metal substrates

*The effect of convection on melt depth was determined in a few sample calculations. The results of these calculations will be qualitatively described.

(aluminum, iron, and nickel) were considered. A description of the Murray and Landis variable-space network technique and the boundary and initial conditions used is presented below, followed by the numerical results obtained using CDC CYBER 175 digital computer. Thermal and physical properties were assumed constant but different for the liquid and solid phases. Data used are listed in Table I.

1) Differential and Difference Equations for a Moving Boundary

The differential equations for one-dimensional heat flow with constant but different thermal properties in the liquid and solid regions are coupled at the liquid-solid interface by

$$k_s \left(\frac{\partial T_s}{\partial X} \right) - k_l \left(\frac{\partial T_l}{\partial X} \right) = \rho H R \quad [1]$$

where R is the velocity of the liquid-solid interface; H is the heat of fusion for the pure metal (negative for melting and positive for solidification); and ρ is the density of the liquid for melting and density of the solid for solidification.

The liquid and solid phases were divided into equally sized space increments which changed in size as the liquid-solid interface moved forward during melting and reversed direction during solidification of the molten layer sometime after the heat flux was removed from the surface. The three point finite difference approximations of the one dimensional heat flow equations and Eq. [1] derived by Murray and Landis¹³ were used.

In all the calculations the distance from the substrate surface to the last nodal point in the solid was large enough so that the temperature of this nodal point remained at the initial temperature of the solid, T_o . This distance was determined by comparing the calculated temperature of the last node to T_o . Finally, trial and error showed that an efficient utilization of computer time without loss of accuracy required 10 increments in the liquid and 20 increments in the solid with the liquid-solid interface located at node No. 11.

2) Boundary and Initial Conditions

The boundary conditions at the surface and last node were determined by carrying out an energy balance across half space increments at these locations.

$$\frac{\partial_{1,m+1} - \partial_{1,m}}{\Delta t} = \frac{2\alpha_l r}{L_m} \left[(\partial_{2,m} - \partial_{1,m}) \frac{r}{L_m} + \frac{q}{k_l} \right] \quad [2]$$

and

$$\frac{\partial_{N,m+1} - \partial_{N,m}}{\Delta t} = \frac{2\alpha_s (N-r)^2}{(E-L_m)^2} (\partial_{N-1,m} - \partial_{N,m}). \quad [3]$$

Equations [2] and [3] are for the surface and the last node, respectively. N is the total number of nodes, r is the number of space increments in the liquid region, L_m is the location of the liquid-solid interface at $r+1$, $\partial = T - T_m$, and E is the location of the last node in the solid.

The additional boundary condition at the liquid solid interface, $X = L_m$, is

$$\partial = T - T_m = 0. \quad [4]$$

Heat loss due to radiation and convection at the metal/air interface was included in the calculations by assuming an effective heat transfer coefficient, h , at this interface an order of magnitude larger than that calculated from radiation only. The term $q_{\text{loss}} = h(T - T_o)$ was incorporated in Eq. [2] above. The magnitude of this heat loss is negligible compared to the absorbed heat fluxes used in our calculations. Hence, the heat loss due to convection and radiation had a negligible effect on the calculated temperature distributions.

When only one phase is present prior to the melting of the solid or at the end of solidification ($L = 0$), terms in the finite difference equations of Murray and Landis¹³ and Eq. [2] above become undefined. Therefore, the melting problem must be started with a small initial value of L and a starting temperature profile in this liquid region must be specified. Similarly, the solution during the solidification half of the program must be stopped before $L = 0$.

A starting procedure similar to that suggested by Heitz and Westwater¹⁴ was especially developed for the specific problem of this investigation. As previously noted temperature distributions for the initial heating of the solid were determined from equations given by Carslaw and Jaeger.¹¹ The solution to these equations was continued until the surface of the solid reached a temperature above the melting temperature of the metal (the solid was superheated). Then the sensible heat of the superheated solid region, $X = X_1$, was instantly converted to heat of fusion, resulting in an initial melt depth, $X = X_2 < X_1$, of uniform temperature, $T = T_m$. The mathematical equivalent of this statement is

$$\rho_s C_{ps} \int_0^{X_1} (T - T_m) dX = \rho_l H X_2. \quad [5]$$

Equation [5] was directly integrated after substituting expressions given in Ref 11. The resulting equation is:

$$\rho_l H X_2 = \rho_s C_{ps} (T_o - T_m) X_1 + q t \left(1 - 4i^2 \operatorname{erfc} \frac{X_1}{2\sqrt{\alpha_s t}} \right). \quad [6]$$

Tabulated values of

$$4i^2 \operatorname{erfc} \frac{X_1}{2\sqrt{\alpha_s t}}$$

are given in Ref. 15.

Figure 2 shows an example of initial temperature distributions established in this way in an aluminum substrate subjected to an absorbed heat flux of 5×10^9 W/m². Curves 2 and 3 in this figure are for the superheated solid and after conversion to an initial melt depth, respectively.

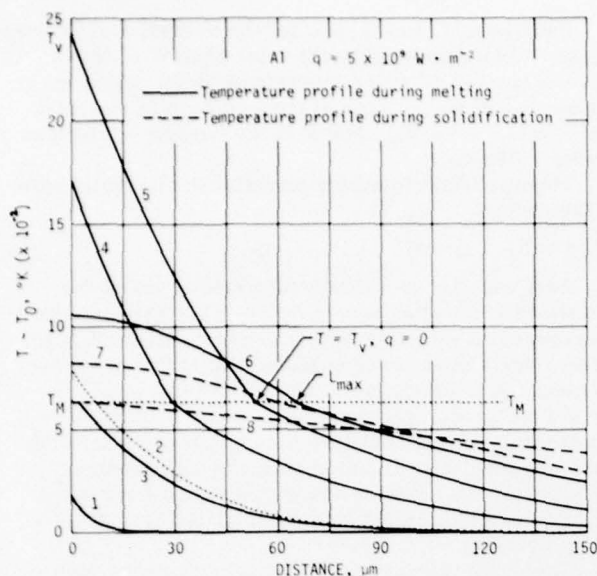


Fig. 2—Temperature distribution in an aluminum substrate at different times during heating of the initial solid, melting and subsequent solidification for an absorbed surface heat flux of $5 \times 10^5 \text{ W/m}^2$. Temperature distributions at successive times are denoted by numbers 1 through 8. Last nodal point in the solid is at a distance of $\sim 600 \mu\text{m}$.

The value of initial melt depth, X_2 , used to start the differential equations was consistently small (between 0.03 and 0.1 of the melt depth). These starting thicknesses were selected to both preserve accuracy of the temperature profiles generated as well as keep solution times required reasonable. Computations were carried out with a time interval continuously determined from $\alpha \Delta t / r^2 / L^2 \approx 1/4$.

The method used to generate initial melt depths of constant temperature $T = T_M$ results in an initial negative interface velocity. However, the melt velocities rapidly change sign and increase to a maximum value over a length of time of approximately 10^{-6} s .

3) Sequence of Numerical Calculations

The sequence of calculations carried out were as follows: Temperature profiles *vs* time were established during heating of the solid until its surface reached and exceeded the melting point of the material. The superheated solid region, X_1 , was converted to initial melt depth, X_2 , using Eq. [5]. Melting was continued until a desired melt depth was reached or until the surface of the liquid layer reached the vaporization temperature of the metal (see curve No. 5 in Fig. 2). The heat flux was removed, $q = 0$ in Eq. [2], and calculations were continued until the interface velocity, R , became negligible*—heat flux in the liquid and

*The interface velocity decreased to a value of approximately three orders of magnitude less than the average for a given power input.

solid at the liquid-solid interface became equal. The melt depth, L (L_{max} when the heat flux was removed at $T_s = T_v$) was thus established (see curve No. 6 in Fig. 2). The sign of the heat of fusion, H , in Eq. [1] was changed to commence solidification (see curves

No. 7 and 8 in Fig. 2). Distance solidified is denoted as ϵ —it is the distance from the melt depth, L , to the location of the liquid-solid interface. Time in all the data presented herein is total time elapsed from initial application of the heat flux to the solid surface.

V. RESULTS OF NUMERICAL CALCULATIONS

The procedure described in the previous section was used to obtain temperature profiles *vs* time, melting, and solidification interface velocities and heating and cooling rates in the surface layers of the three metals (aluminum, iron, and nickel). Results of this work are presented in a general enough form to permit determination of most of these variables for large ranges of absorbed heat fluxes and times.

Calculated melt depths *vs* total time for several absorbed heat fluxes are shown in Fig. 3. The arrows in the figure denote times at which the surface of each material reaches its vaporization temperature and the heat flux, q , is removed. As noted earlier, melting continues a while longer until a maximum melt depth, L_{max} , is reached. Maximum melt depths *vs* absorbed heat flux calculated via numerical techniques are plotted in Fig. 1 for comparison with those predicted using the integral profile technique. Melt depth during the melting and subsequent solidification periods can also be expressed in dimensionless form, $\rho_s H L / q t_m$. Figure 4 shows this function plotted *vs* dimensionless time, t/t_m , for the three elements. The maxima in the bell-shaped curves correspond to maximum melt depths, L_{max} .

The ratios of melt depth to maximum melt depth, L/L_{max} , are plotted *vs* $q\sqrt{t}$ for the three materials in Fig. 5. On the right-hand side of Fig. 5, data are presented to permit determination of distance from the interface to the last nodal point in the solid, S , at any time during melting or solidification. The total distance from the surface of the metal to the last nodal point in the solid is $E = S + L$; it is a constant at a given absorbed heat flux. For example, an aluminum substrate absorbing a heat flux of $q = 5 \times 10^5 \text{ W/m}^2$

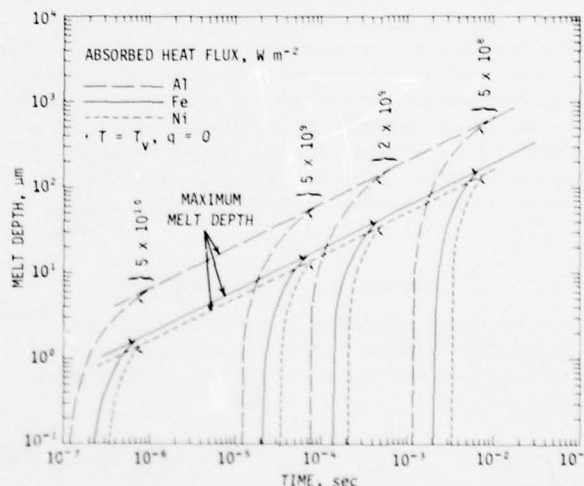


Fig. 3—Melt depth *vs* total time for different absorbed heat fluxes obtained via the numerical technique. Arrows indicate times at which a surface reaches its vaporization temperature and heat flux is removed.

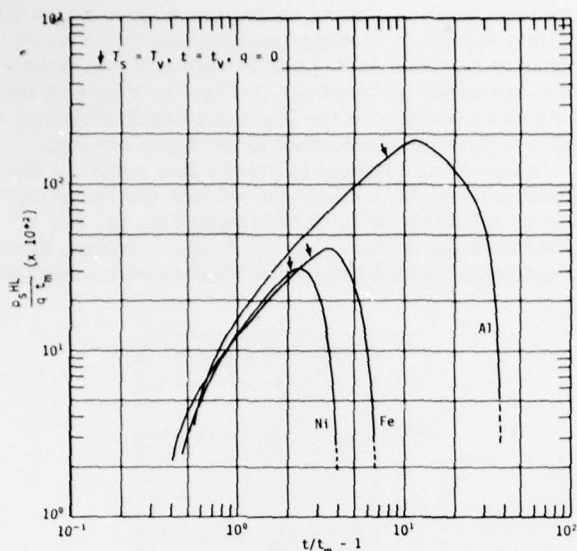


Fig. 4—Dimensionless melt depth $\rho_s H L / q \sqrt{t_m}$ during melting and solidification vs dimensionless time, t/t_m .

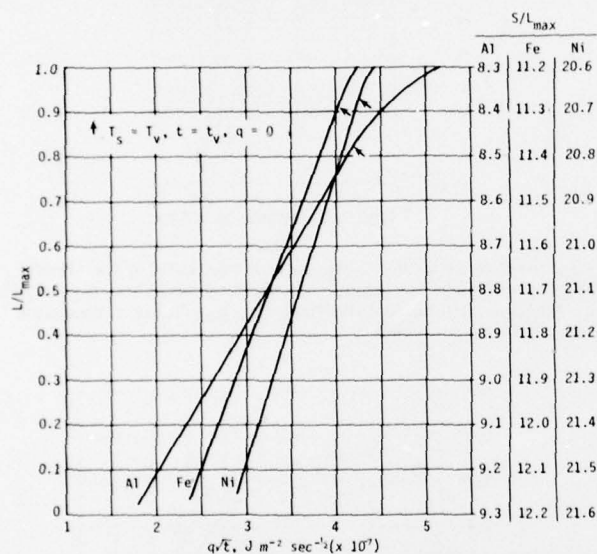


Fig. 5—Dimensionless melt depth, L/L_{max} , and dimensionless distance from the liquid-solid interface to the last nodal point in the solid vs $q\sqrt{t}$ for aluminum, iron and nickel substrates.

will achieve a maximum melt depth of approximately $65 \mu m$ at a time of $t_{max} \approx 1.08 \times 10^{-4} s$. The value of S at this time, $L/L_{max} = 1.0$, is obtained from Fig. 5; $S/L_{max} = 8.3$, $S \approx 535 \mu m$. Therefore, the distance from the surface of the metal to the last nodal point is $E \approx 600 \mu m$. Using the curves and the right-hand data presented in Fig. 5, the melt depth and the heat affected zone in the solid, S , can be determined any time during the melting and the solidification period.

The information generated above permits determination of the location of each nodal point during melting and solidification. The temperature profiles in the two phases throughout the melting process and during solidification after reaching a maximum melt depth can thus be established from Figs. 6, 7, and 8.

As expected, there is significant loss of superheat from the liquid region during the time period $t_v \leq t \leq t_{max}$. On the other hand, the solid portion of the substrate heats up continuously during the melting and solidification cycles.

Interface velocity, R , is directly proportional to the absorbed heat flux. R/q vs fractional distance melted or solidified, X/L_{max} , for the three substrates are shown in Fig. 9. X denotes melt depth, L , during melting and distance solidified, ϵ , during solidification. The change in temperature with time in the liquid at

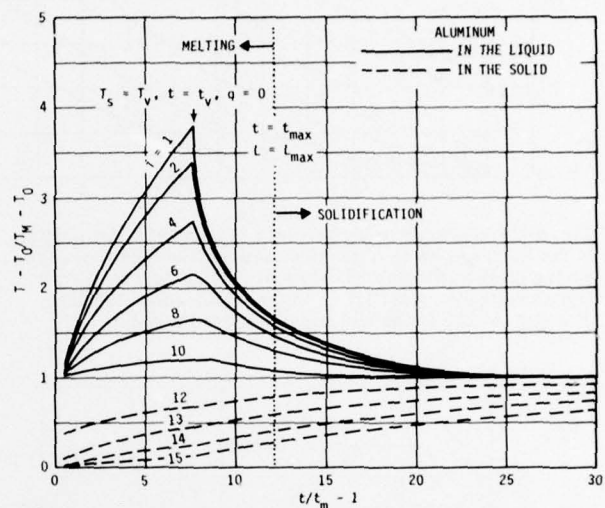


Fig. 6—Dimensionless temperature at each nodal point in the liquid and the solid regions as a function of dimensionless time, t/t_m , during melting and solidification of the surface layer of an aluminum substrate. $i = 1$ is the nodal point located at the surface and $i = 31$ is the last nodal point in the solid.

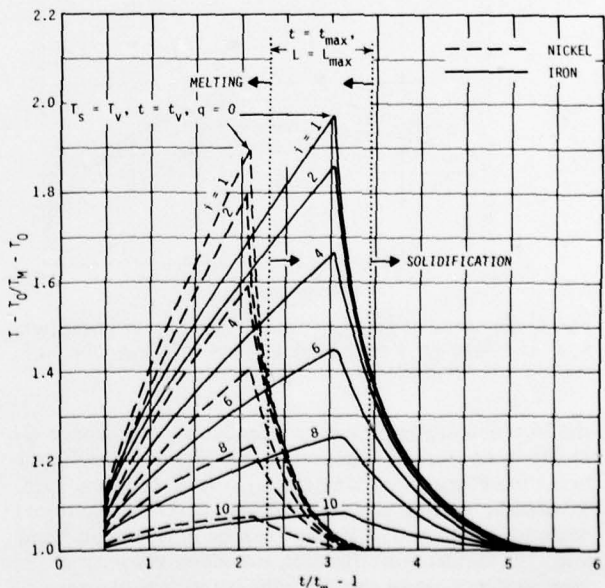


Fig. 7—Dimensionless temperatures at each nodal point in the liquid regions as a function of dimensionless time, t/t_m , during melting and solidification of surface layers of iron and nickel substrates. $i = 1$ is the nodal point located at the surface.

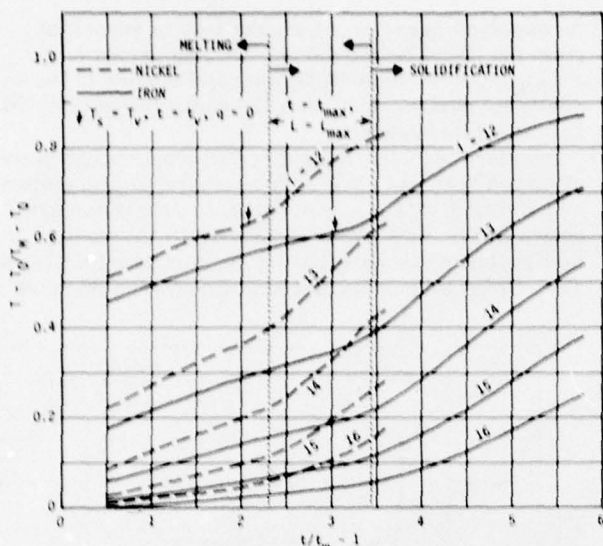


Fig. 8—Dimensionless temperature at several nodal points in the solid region as a function of dimensionless time, t/t_m , during melting and solidification of surface layers of iron and nickel substrates. $i = 11$ is the liquid-solid interface, $T = T_M$. $i = 31$ is the last nodal point in the solid.

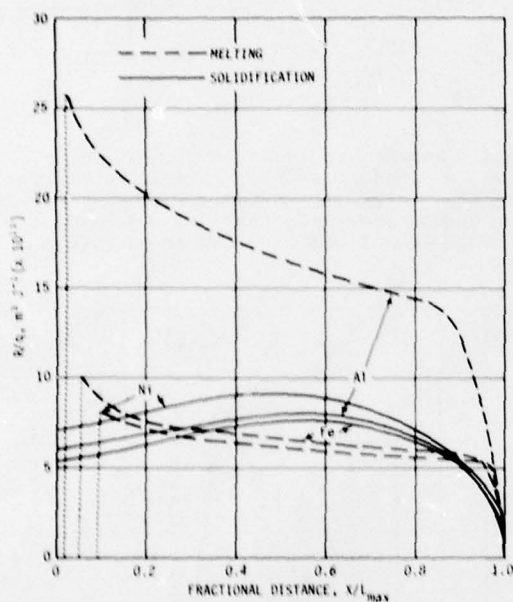


Fig. 9—The ratio of interface velocity to absorbed heat flux, R/q , as a function of fractional distance, X/L_{\max} , during melting and solidification.

the liquid-solid interface is equal to $G_L \cdot R$ where G_L is the temperature gradient in the liquid at the liquid-solid interface. The function $G_L \cdot R/q^2$ (cooling rate divided by square of absorbed heat flux) vs fractional distance solidified, ϵ/L_{\max} , can be determined from Fig. 10. Initial solidification interface velocity is zero but increases rapidly with fractional distance solidified; that is, on an expanded ϵ/L_{\max} scale, the curves in Fig. 10 pass through the origin. As noted from the temperature profiles presented in Figs. 2, 6, and 7, all the superheat in the liquid is lost ($G_L \cdot R$

becomes zero) sometime before the surface layer completely solidifies. Average cooling rate in the liquid phase at any time during solidification vs fractional distance solidified as shown in Fig. 11. This cooling rate is a maximum at the beginning of solidification when temperature gradients in the liquid are high.

Temperature gradient to growth rate ratios vs fractional melt depth, L/L_{\max} for various fractional distances solidified, ϵ/L , are shown in Fig. 12. For a given melt depth, L/L_{\max} , G_L/R is a maximum at the beginning of solidification and drops to zero sometime

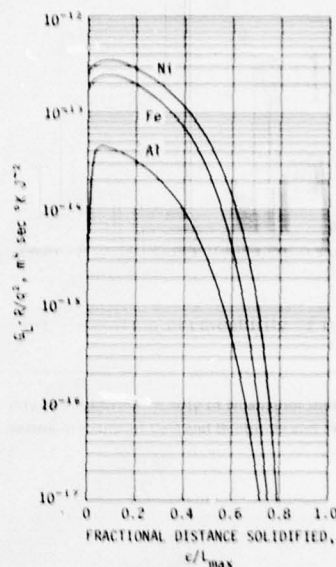


Fig. 10—The ratio of cooling rate in the liquid at the liquid-solid interface to the square of absorbed heat flux, $G_L \cdot R/q^2$, vs fractional distance solidified, ϵ/L_{\max} , after a maximum melt depth is achieved.

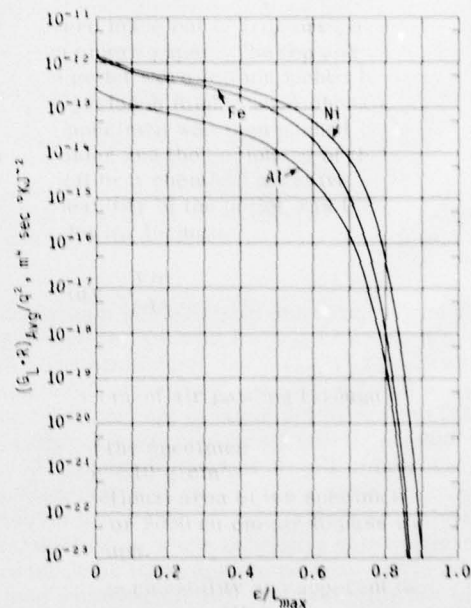


Fig. 11—The ratio of average cooling rate in the liquid to the square of absorbed heat flux, $(G_L \cdot R)_{\text{Avg}}/q^2$ vs fractional distance solidified, ϵ/L_{\max} .

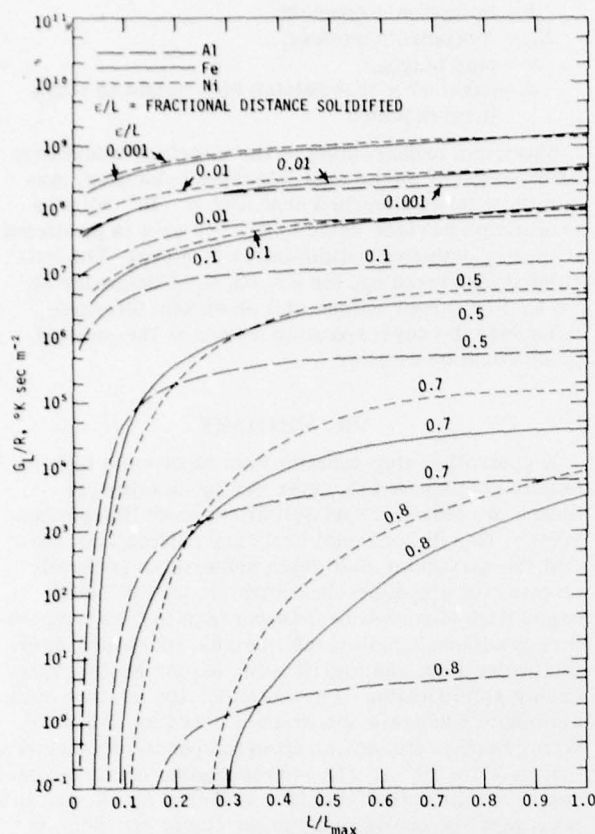


Fig. 12—Temperature gradient to growth rate ratio at the liquid-solid interface, G_L/R , vs fractional melt depth, L/L_{\max} , for various fractional distances solidified, ϵ/L .

near the end of solidification as superheat in the liquid is lost. Data in Fig. 12 also show that G_L/R increases as melt depth approaches the maximum melt depth, $L/L_{\max} \rightarrow 1.0$.

Finally, cooling rates for solidification of noncrystalline structures were calculated by setting the heat of fusion, H , equal to zero (see Fig. 13). Total average cooling rate was obtained by averaging over melt depth and temperature until the surface reached one-half of the melting temperature.

VI. DISCUSSION

The important influence of high cooling rates on refinement of solidification microstructure, increased solid solubility, formation of nonequilibrium crystalline and noncrystalline phases has now been well established. Yet, direct correlation of temperature profiles during solidification with microstructure has been hampered due to experimental difficulties. The availability and continuous development of high intensity power sources such as CO_2 laser may alleviate these problems in due course. First, surface melting experiments carried out under controlled conditions would lead to predictable melt depths in intimate contact with the substrate below. These are two important variables that cannot be controlled in splat cooling. Second, variation in heat flux would permit directional solidification under a variety of temperature gradient

and growth rate conditions. Finally, isolation of growth from nucleation coupled to experimental techniques yet to be developed for accurate temperature measurements would greatly enhance our fundamental understanding of rapid solidification phenomena.

The results presented above show the significant range of melting and solidification variables that are available with variation of absorbed heat flux when heat flow is construed to be unidirectional. The general trends established in this study are summarized in Table II.

When the Absorbed Heat Flux is Increased by an Order of Magnitude, the Following Effects are Noted on the Other Variables:

a) Time. The various times, t_m , t_v , and t_{\max} decrease by two orders of magnitude. In general, the surface of a material reaches a given temperature when $q\sqrt{t}$ is kept constant. The significance of this finding is that at higher power inputs, less time is available for diffusion of heat into the metal substrate—absorbed heat is concentrated near the surface of the material leading to steeper temperature gradients.

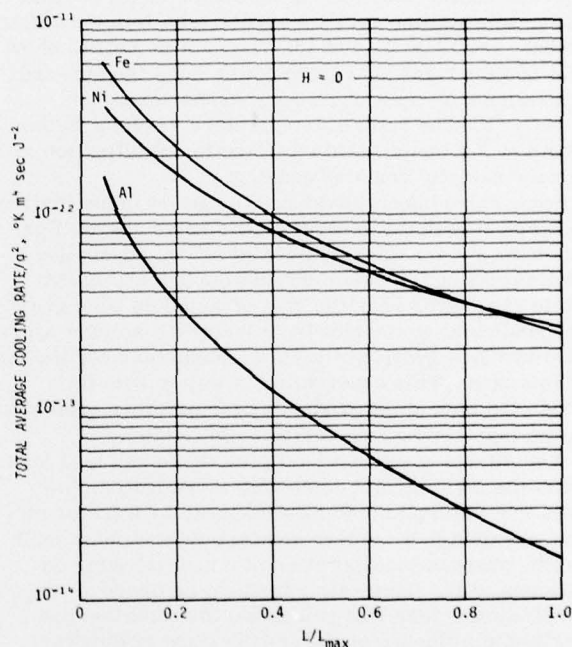


Fig. 13—The ratio of total average cooling rate to the square of absorbed heat flux vs fractional distance melted, L/L_{\max} , during solidification of a noncrystalline solid.

Table II. The Effect of Change in Absorbed Heat Flux on Other Variables

Order of magnitude increase in q results in the following changes						
q	Time	Melt Depth	R	G_L	$G_L \cdot R$	G_L/R
10^\dagger	$10^2 \downarrow$	$10 \downarrow$	10^\dagger	10^\dagger	$10^2 \uparrow$	\leftrightarrow
\dagger increase						
\downarrow decrease						
\leftrightarrow no change						

b) **Melt Depth.** The melt depth decreases by one order of magnitude—it is inversely proportional to the absorbed heat flux. As an example, note that the slope of plots of maximum melt depth *vs* absorbed heat flux on a log-log plot (Fig. 1) is -1. The general forms of this finding are presented in Figs. 4 and 5. Figure 4 shows that for a given substrate material, the dimensionless melt depth, $\rho_s HL/q t_m$, during melting and subsequent solidification is a constant at a given dimensionless time, t/t_m . Or, for a given $q\sqrt{t}$, the dimensionless melt depth, L/L_{\max} , is a constant, see Fig. 5.

c) **Temperature Gradient.** The temperature gradients in the liquid and the solid regions increase by an order of magnitude. This fact is illustrated in Figs. 6, 7, and 8 where the temperature distributions are presented in terms of dimensionless temperature at each nodal position.

d) **Interface Velocity.** The interface velocity both during melting and solidification increase by an order of magnitude. This fact can be directly deduced from the above and is illustrated in Fig. 9.

e) **Cooling Rates.** Cooling rates in the liquid at the liquid-solid interface, $G_L \cdot R$, during solidification increase by two orders of magnitude, see Fig. 10. Average cooling rate in the liquid region and total average cooling rate during formation of crystalline and noncrystalline solids, respectively, follow similar trends, see Figs. 11 and 13. The data in Fig. 13 show that cooling rates at a given power input tend toward a maximum as melt depth approaches zero.

f) G_L/R . The ratio of temperature gradient in the liquid at the liquid-solid interface to solidification interface velocity remains constant.

Some experimental evidence to date is in qualitative agreement with the general trends noted above. For example, recent work by Beck *et al*¹⁶ on superalloy melts produced by laser irradiation has shown that while structures near the root of a molten zone grow perpendicular to the substrate material, solidification also involves growth of parallel dendrites near the top of this zone. This observation is in line with the predicted loss of perpendicular temperature gradients in the liquid sometime during solidification.

The effects of convection in the liquid and heat loss from the melt surface were also investigated. Increasing the liquid metal conductivity by a factor of five resulted in a similar increase in maximum melt depth, whereas incorporation of a heat transfer coefficient at the liquid/air interface, an order of magnitude larger than that calculated for radiation had negligible influence on the temperature gradients.

Finally, kinetic limitations to melting and solidification are not expected to significantly effect the calculated temperature distributions. If we assume that both melting and solidification occur in the continuous regime as discussed by Cahn *et al*¹⁷ then the following equation is applicable.

$$R = \frac{\beta D_L H \Delta T}{\alpha k N_o T M^2} \quad [7]$$

where:

ΔT = superheat or undercooling at the interface during melting and solidification, respectively,

k = Boltzman's constant,

N_o = Avagadro's number,

α = step height,

β = parameter that relates step height to mean jump distance.

Maximum undercooling at the interface would thus be expected at the highest interface velocities. Assuming a large absorbed heat flux of $\sim 10^{10}$ W/m² a maximum interface velocity of ~ 0.9 m/s is predicted from Fig. 9 during solidification of nickel. The calculated undercooling, for $\beta \approx 60$, is of the order of ~ 6 K. For larger values of β or slower interface velocities the corresponding change in the melting point would be smaller.

VII. SUMMARY

A controlled step-function heat input via a high intensity continuous CO₂ laser can be an effective means of studying rapid solidification of thin surface layers. One dimensional heat flow calculations show that the maximum melt depth achieved is generally an order of magnitude less than the heat affected zone. High absorbed heat fluxes lead to high temperature gradients, shallow melt depths, increased interface velocities, and significantly higher cooling rates during solidification. For example, the surface of an aluminum substrate absorbing a heat flux of 5×10^9 W/m² reaches its vaporization temperature in approximately 7.1×10^{-5} s. The corresponding maximum melt depth, solidification interface velocity, G_L/R , and maximum average cooling rate in the liquid are $\sim 65 \mu\text{m}$, ~ 0.45 m/s, 3×10^8 K s/m, and 6.5×10^6 K/s, respectively. For the same power input, a melt depth of approximately $14.2 \mu\text{m}$ is achieved in approximately 2.42×10^{-5} s; the corresponding total average cooling rate for noncrystalline solidification of this melt is approximately 7.5×10^6 K/s.

NOMENCLATURE

C_p	specific heat, J kg ⁻¹ K ⁻¹ ,
E	distance from the surface to the last nodal point in the solid, m or μm ,
G	temperature gradient, K m ⁻¹ ,
G_L	temperature gradient in the liquid at the liquid-solid interface, K m ⁻¹ ,
H	heat of fusion, J kg ⁻¹ ,
k	thermal conductivity, J s ⁻¹ m ⁻¹ K ⁻¹ ,
L	melt depth, m or μm ,
L_{\max}	maximum melt depth achieved after heat flux is removed when the surface reaches the vaporization temperature of the material, m or μm ,
L/L_{\max}	dimensionless melt depth,
$\rho_s HL/q t_m$	dimensionless melt depth,
n	increments of space, dimensionless
N	total number of space increments, dimensionless,
q	absorbed heat flux, w/m ² ,
r	number of space increments in the liquid region, dimensionless,
R	interface velocity, m s ⁻¹ ,
S	distance from the liquid-solid interface to the last nodal point in the solid, m or μm ,

t	total time after application of heat flux, s,
t_m	time for the surface of a material to reach its melting temperature, s,
t_{\max}	time for a material to achieve a maximum melt depth, s,
t_v	time for surface of a material to reach its vaporization temperature, s,
T	temperature, K,
T_o	ambient temperature, K,
T_M	melting temperature, K,
T_s	surface temperature, K,
T_v	vaporization temperature, K,
X	distance from the surface, m or μm ,
α	thermal diffusivity = $k/\rho C_p$, $\text{m}^2 \text{s}^{-1}$,
ϵ	position of solidification interface measured from melt depth, L , m or μm ,
$\theta = T - T_M$	temperature excess above the melting temperature, K,
$\theta_{n,m}$	temperature excess at space point n , time point m , K,
ρ	density, kg m^{-3} .

Subscripts

l	liquid material,
s	solid material.

ACKNOWLEDGMENTS

A portion of this work was sponsored by the Defense Advanced Research Projects Agency. Technical dis-

cussions with Professor G. J. Abbaschian on the kinetic limitation of growth rate are gratefully acknowledged.

REFERENCES

1. P. Duwez, R. H. Willens, and W. Klement: *J. Appl. Phys.*, 1960, vol. 31, pp. 1136.
2. P. Duwez: *Techniques of Metal Research*, R. F. Bunshah, ed., Interscience, New York, 1968, p. 347.
3. P. Predecki, A. W. Mellendore, and N. J. Grant: *Trans. TMS-AIME*, 1965, vol. 233, p. 1581.
4. D. R. Harbur, J. W. Anderson, and W. J. Mateman: *Trans. TMS-AIME*, 1969, vol. 245, p. 1055.
5. E. M. Breinan, B. H. Kear, C. M. Banas, and L. A. Greenwald: *Proc., Third International Symposium*, Seven Springs, Penn.; B. H. Kear, D. K. Murjka, J. K. Tein, and S. T. Vlodak, Clator's Publishing Div., Baton Rouge, La., 12-15 September 1976, p. 435.
6. M. I. Cohen: *J. Franklin Inst.*, 1967, vol. 283, no. 4, p. 271.
7. G. H. Harth, W. C. Leslie, V. G. Gregson, and B. A. Sanders: *J. Metals*, April 1976, p. 5.
8. D. Rosenthal: *Weld J.*, 1941, vol. 20, Research Supplement, p. 220S.
9. H. G. Landau: *Quart. Appl. Math.*, 1950, vol. 8, no. 1, p. 81.
10. T. R. Goodman: *Advances in Heat Transfer*, T. F. Irvine and J. P. Hartnett, eds., 1964, vol. 1, p. 51.
11. H. S. Carslaw and J. C. Jaeger: *Conduction of Heat in Solids*, Oxford University Press, Second Edition, 1973.
12. G. W. Evans, E. Isaacson, and J. K. L. MacDonald: *Quart. Appl. Math.*, 1950, vol. 8, p. 312.
13. W. D. Murray and F. Landis: *Trans., ASME*, 1959, vol. 81, p. 106.
14. W. L. Heitz and J. W. Westwater: *Int. J. of Heat and Mass Transfer*, 1970, vol. 13, p. 1375.
15. J. Kaye: *J. Math. Phys.*, 1955, vol. 34, p. 119.
16. D. Beck, S. M. Copley, M. Bass, and E. Van Stryland: *Proceedings of Conference on Rapid Solidification Processing Principles and Technologies*, Reston, Virginia, Nov. 13-16, 1977, to be published.
17. J. W. Cahn, W. B. Hilling, and G. W. Sears: *Acta Met.*, 1964, vol. 12, p. 1421.